Fast Track

Kang Ping Chen[1,2]
Jose Rafael Pacheco[1,3]
Mark. A. Hayes[4]
Sarah J. R. Staton[4]

[1]Department of Mechanical and Aerospace Engineering, Arizona State University, Tempe, AZ, USA
[2]College of Petroleum Engineering, China University of Petroleum, Beijing, P. R. China
[3]Center for Environmental Fluid Dynamics, Arizona State University, Tempe, AZ, USA
[4]Department of Chemistry and Biochemistry and Center for Solid State Electronics Research, Arizona State University, Tempe, AZ, USA

Received December 22, 2008
Revised December 22, 2008
Accepted February 12, 2009

Research Article

Insulator-based dielectrophoretic separation of small particles in a sawtooth channel

Insulator-based dielectrophoretic separation of small particles in a sawtooth channel is studied in the limit of dilute concentration. Pathlines for the movements of infinitesimal particles are constructed and the geometric changes of these pathlines are used to establish the criterion for blocking and trapping particles with different physical properties. The sharp corners of the sawtooth channel create much stronger dielectrophoretic force than channels with smooth corners for blocking particle movements. Particle blocking and trapping depend on particle properties and the geometry of the device. It is shown that once the channel geometric aspect ratios are specified, the blocking criterion depends on only a single dimensionless parameter C defined in terms of the particle mobility ratio (dielectrophoretic *versus* electrokinetic), the applied voltage and the spacing between the teeth. Selective blocking and trapping of particles can be realized by varying the geometry of the channel progressively. High-resolution separation can be achieved by tuning the differential in the parameter C to a desired level.

Keywords:
Dielectrophoresis / Particle trapping / Separation DOI 10.1002/elps.200800833

1 Introduction

There is growing interest in developing efficient, high-resolution techniques for separating mixtures of complex biological particles and structures. Much of the recent work has focused on developing electric-field-based microfluidic separation devices. These devices are particularly attractive due to their promise of high separation efficiencies, short analysis times and minimal sample consumption. Most of the currently employed methods rely on either electrophoretic force for linear separations or dielectrophoretic force for bifurcation strategies. However, enhanced and unique capabilities can be achieved by utilizing the effects of both forces in a linear separation mode. Growing from the work of Pohl [1], dielectrophoresis (DEP) can be used as a counter force to achieve local equilibrium. In this mode, DEP-based forces trap particles by countering bulk particle motion, which can be induced by pressure-driven flow, electroosmosis, electrophoresis or a combination of the three, with local dielectrophoretic forces. Dielectrophoretic force is exerted by a non-uniform electric field on a polarizable particle, which depends on the dielectric properties of the particle and the suspending medium. Since the dielectric properties of a particle are a function of both its structure and composition, DEP-based techniques access a much richer set of particle properties than electrophoresis [1–7]. This feature enables DEP-based techniques to offer electrically controllable trapping, focusing, translation, fractionation and characterization of particles within a fluid suspending medium with enhanced selectivity and sensitivity (Fig. 1). Impressive results have been achieved with DEP-based separation, including separating cancer cells from blood cells [8–11], parasitized cells from normal cells [10–23], and live from dead cells [14].

The work presented here is in distinct contrast with the widely used electrode-based DEP separation, which relies on the high electric fields and field gradients created by the embedded electrodes with a relatively low applied potential. There are a variety of inherent limitations with the electrode-based system. One is that the electrodes used to establish the required non-uniform electric field are embedded within the separation chamber. These can cause undesirable electro-chemical reactions and gas generation at the surfaces

Correspondence: Professor Kang Ping Chen, Department of Mechanical and Aerospace Engineering, Arizona State University, Tempe, AZ 85287-6106, USA
E-mail: k.p.chen@asu.edu
Fax: +1-480-965-1384

Abbreviations: DEP, dielectrophoresis; **iDEP,** insulator-based DEP

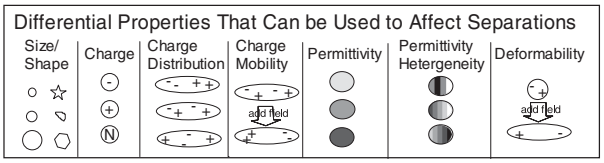

Figure 1. A list of particle properties that can affect separations.

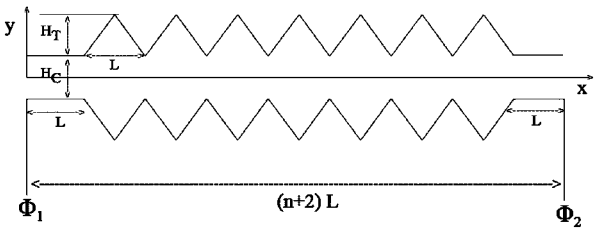

Figure 2. A non-converging sawtooth-shape channel with n teeth. In this study $n = 7$. The channel walls are insulated.

of these electrodes. Although the use of AC rather than DC voltage helps to minimize these effects, it does not eliminate them. Traditional DEP separation devices of this kind are also generally limited to separating two distinctly different components, one that collects in the high field strength regions (typically located on, or near, the electrodes) and one that does not. Consequently, separating particles with similar properties requires optimizing the specific experimental parameters, such as buffer conductivity, field strength and frequency. Various techniques have emerged in response to these limitations [23–29].

More recently, insulator-based DEP (DC-iDEP) has emerged [30–39]. This method differs from traditional DEP separation in that a DC voltage is applied to electrodes located in remote inlet and outlet reservoirs and the field non-uniformities are generated by arrays of insulating posts located within the channel. Cummings and Singh [30] described a theoretical basis of the technique and demonstrated proof-of-principle using latex spheres. In subsequent studies, the technique was used to concentrate and isolate live and dead bacteria [31, 33]. Geometric shapes were exploited for bacteria separation from latex particles [34]. DC-iDEP offers several advantages compared with traditional DEP. The use of remote electrodes avoids many of the problems associated with embedded electrodes, such as electrochemical reactions and gas generation at the electrode surfaces. Additionally, the field can be generated by applying DC rather than AC voltage. The use of a DC field can be advantageous because it can be used to drive both electrophoretic and dielectrophoretic transports, allowing greater control over particle movement.

Pysher and Hayes [39] recently developed a new DC-iDEP device with a converging sawtooth microchannel for separating mixtures of bioparticles and demonstrated proof-of-principle using bacteria cells as a model system for separating biological structures. The geometry of the converging sawtooth channel allows controlled variation of the gradient of electric field strength and thus the strength of the DEP force acting on the particles. Electrophoresis and electroosmosis are used to transport the particles through this channel containing a series of progressively stronger field gradient regions. As the particles are transported through the channel, they are isolated according to their characteristic physical properties in response to electrophoretic and dielectrophoretic forces. The promising results obtained in their work suggest that the technique may form the basis for a highly versatile and useful tool for separating biological particles. To this end, we study in this paper the particle transport and separation mechanism in detail for a sawtooth channel. To focus on particle behavior and to simplify analysis, the channel is here assumed to be non-converging with seven identical teeth (Fig. 2). This unit of non-converging sawtooth channel can be used as a basic building block to construct a separation device. Although particle interaction and aggregation are important for separation efficiency, this study is limited to a single infinitesimal particle, since the motion of a single particle in a DC-iDEP device is still not fully understood. Some salient features of particle motion are revealed and criteria are established for particle blocking and trapping in this device in terms of a dimensionless parameter, which involves an electrophoretic and dielectrophoretic mobility ratio, the applied voltage and the spacing between the teeth.

2 Motion of an infinitesimal particle suspended in an electrolyte solution

Consider the motion of a small charged particle in a dielectric fluid under the influence of a DC electric field in a sawtooth-shaped channel (Fig. 2). The electric field is generated by two remote electrodes just outside the channel, and the channel walls are insulated. Assuming the particle size is much smaller than the length scale of the spatial variation of the electric field, the point-dipole model [6] can be applied and the dielectrophoretic force acting on a particle can be expressed in terms of the electric field unperturbed by the presence of the particle. If the electric double layer formed around the particle is thin compared with the size of the particle, then the translational velocity of the particle is governed by Newton's second law:

$$m_p \frac{d\mathbf{v}_p}{dt} = -6\pi\eta a(\mathbf{v}_p - \mathbf{u}) + q\mathbf{E} + 4\pi\varepsilon_f a^3 \beta(\mathbf{E}\cdot\nabla)\mathbf{E} \qquad (1)$$

where $\mathbf{v}_p$ is the instantaneous particle velocity in an inertial frame of reference, $\mathbf{u}$ is the velocity of the fluid, $\mathbf{E}$ is the unperturbed electric field. In (1), m_p is the mass of the particle, q the charge on the particle, and η and ε_f are the viscosity and permittivity of the suspending fluid, respectively. β is the Clausius–Mossotti factor, which in the DC limit for a dielectric particle is given by $\beta = \varepsilon_p - \varepsilon_f/\varepsilon_p + 2\varepsilon_f$, where ε_p is the permittivity of the particle [6]. Positive DEP (movement toward field maxima) occurs if a particle is more polarizable than the medium ($\beta > 0$), whereas negative DEP (movement toward field minima) occurs if a particle is less polarizable ($\beta < 0$). For simplicity, the particle is assumed to be spherical with a radius of a. The first term on the right-hand side of

Eq. (1) is the Stokes drag on the particle due to the viscous fluid; the second and third terms represent the electrophoretic force and the dielectrophoretic force acting on the particle, respectively. This equation is also valid in the dilute particle concentration limit, so long as the inter-particle separation r is large, since the particle–particle interactions decay as $1/r^5$ [40]. When these conditions are not satisfied, however, the perturbed electric field has to be computed, and the forces acting on the particle can be obtained from the integration of the Maxwell stress tensor [41].

With the above assumptions, the particle velocity $\mathbf{v}_p$ can be found in terms of the local fields by integrating Eq. (1). Typically a particle reaches its terminal velocity in the order of 10^{-4} s, and the particle moves with its terminal velocity (this is equivalent to the statement that particle inertial effect is negligible):

$$\begin{aligned}\mathbf{v}_p &= \mathbf{u} + \mu_{EM}\mathbf{E} - \mu_{DEP}(\mathbf{E}\cdot\nabla)\mathbf{E} \\ &= \mathbf{u} + \mu_{EM}\mathbf{E} - \frac{\mu_{DEP}}{2}\nabla|\mathbf{E}|^2\end{aligned} \tag{2}$$

where $\mu_{EM}=q/6\pi\eta a$ is the particle electrophoretic mobility, and $\mu_{DEP}=-2\varepsilon_f a^2\beta/3\eta$ (>0, for negative DEP) is the particle dielectrophoretic mobility. For definitiveness, we assume that the electrode near the channel entrance has a higher potential so that the electric current flows from left to right. Thus only particles with positive charge ($q>0$) can enter the channel. This also implies that $\mu_{EM}>0$.

The fluid velocity in the channel is electroosmotic: $\mathbf{u}=\mu_{EO}\mathbf{E}$ with $\mu_{EO}=\varepsilon_f\varsigma_w/\eta$ being the electroosmotic mobility, ς_w the zeta-potential on the wall, and $\mathbf{E}$ the local electric field. We shall assume $\varsigma_w>0$ so that both fluid electroosmosis and particle electrophoresis drive the motion of the particle from the entrance to the exit as shown in Fig. 2. The particle velocity (2) can be expressed as

$$\begin{aligned}\mathbf{v}_p &= \frac{d\mathbf{r}_p}{dt} = (\mu_{EO}+\mu_{EM})\mathbf{E} - \mu_{DEP}(\mathbf{E}\cdot\nabla)\mathbf{E} \\ &= (\mu_{EO}+\mu_{EM})E\mathbf{e}_t - \mu_{DEP}E\frac{\partial}{\partial s}(E\mathbf{e}_t) \\ &= E(\mu_{EO}+\mu_{EM}-\mu_{DEP}\frac{\partial E}{\partial s})\mathbf{e}_t + \frac{\mu_{DEP}E^2}{R}\mathbf{e}_n\end{aligned} \tag{3}$$

In (3), $\mathbf{r}_p = x_p\mathbf{i}+y_p\mathbf{j}$ is the particle position vector, ($\mathbf{e}_t$, $\mathbf{e}_n$) are the unit tangential vector and unit normal vector on the electric field line, with $\mathbf{e}_n$ pointing away from the center of curvature. s is the arc-length along the electric field line and R is the radius of curvature of the electric field line. Clearly when the electric field lines are curved, the particle no longer moves along the electric field line when dielectrophoretic effect is present.

The axial velocity (horizontal) of the particle is given by

$$\begin{aligned}U_p &= \mathbf{v}_p\cdot\mathbf{i} = E\left(\mu_{EO}+\mu_{EM}-\mu_{DEP}\frac{\partial E}{\partial s}\right)\mathbf{e}_t\cdot\mathbf{i} + \frac{\mu_{DEP}E^2}{R}\mathbf{e}_n\cdot\mathbf{i} \\ &= E\left(\mu_{EO}+\mu_{EM}-\mu_{DEP}\frac{\partial E}{\partial s}\right)\cos\theta - \frac{\mu_{DEP}E^2}{R}\sin\theta\end{aligned} \tag{4}$$

where θ is the angle between the tangent on the electric field line and the x-axis. The two terms with negative signs in U_p are due to dielectrophoretic force. Thus the axial particle velocity is determined by the local electric field line properties. If the electric field line is locally straight, then $R=\infty$, and the sine term is identically zero. Only in this case a particle will travel along the electric field line. The statement that the flux along the electric field lines needs to be zero in order to trap particles [31, 32] is incorrect when the electric field lines are curved, as particle motions do not follow the electric field lines. In fact, U_p becomes zero at a certain cross-section of the channel is only a *necessary* condition for blocking particles. It will be demonstrated in Section 4 that the existence of a reverse velocity zone is sufficient to block the movements of particles.

3 Trajectories of infinitesimal particles in a sawtooth channel

3.1 The electric field and particle trajectories

The electric potential ϕ satisfies the Laplace equation

$$\nabla^2\phi = 0 \tag{5}$$

outside the electric double layers and the electric field is given by $\mathbf{E}=-\nabla\phi$. Since ϕ is the solution to a Laplace equation, the extrema of ϕ can occur only on the domain boundaries.

We prescribe the differential in the values of the electric potential at the two electrode is $\Delta\Phi_0$, and the apparent electric intensity is $E_{app}=\Delta\Phi_0/(n+2)L$, with $n=7$ being the number of teeth and L the spacing between the tips of two adjacent teeth. To make the problem dimensionless, we scale length with L and the electric potential with $\Delta\Phi_0$. Then the following parameters emerge:

$$\begin{aligned}E_{app} &= \frac{\Delta\Phi_0}{(n+2)L} = \frac{\Delta\Phi_0}{9L} \text{ (apparent electric intensity)} \\ h_T &= \frac{H_T}{L} \\ h_C &= \frac{H_C}{L}\end{aligned} \tag{6}$$

The *dimensional* electric field strength $\tilde{\mathbf{E}}$ is related to the computed dimensionless electric field $\boldsymbol{E}$ by the relation $\tilde{\mathbf{E}}=\frac{\Delta\Phi_0}{L}\mathbf{E}=(n+2)\mathbf{E}_{app}\mathbf{E}=9E_{app}\mathbf{E}$.

The advantage of using the point-dipole model [6] is that once the electric field is determined, the particle velocity is given by Eq. (3). The particle trajectory can be determined by integrating its velocity $\mathbf{v}_p$ over time for a given initial particle position from Eq. (3). Thus by plotting all pathlines $y_p=y_p(x_p)$, the trajectories of particles can be readily determined from their initial positions upstream at the entrance of the channel.

If we scale the particle velocity with $(\mu_{EO}+\mu_{EM})\Delta\Phi_0/L$, the dimensionless particle velocity is then given by

$$\mathbf{v}_p = \mathbf{E} - C(\mathbf{E}\cdot\nabla)\mathbf{E} \tag{7}$$

where

$$C = \frac{\mu_{DEP}}{\mu_{EO}+\mu_{EM}} \frac{\Delta\Phi_0}{L^2} = \lambda \frac{\Delta\Phi_0}{L^2} \quad (8)$$

In (7), we have kept the same notations as before, but the particle velocity, the electric intensity and the gradient operator in (7) are all dimensionless. Thus, once the geometry of the channel is specified *via* parameters h_T, h_C and n the velocity of the particle, the pathline of the particle is controlled by the dimensionless parameter C and the initial position of the particle. Note that the parameter C can be altered independently by the mobility ratio $\lambda=\mu_{DEP}/\mu_{EO}+\mu_{EM}$, the applied voltage across the channel $\Delta\Phi_0$ and the dimension of the width of the teeth L. These three factors can be used effectively to manipulate the movement of a particle within a sawtooth channel.

A non-staggered non-uniform grid layout is employed to solve the Laplace equation (3) with a multigrid method. Readers may consult Pacheco [42] and Pacheco and Peck [43] for more in-depth technical details on the computational technique.

3.2 Particle behavior near a sharp corner

Early studies using insulated DEP have used diamond-shaped insulator posts in the interior to create gradients in the electric field [30, 31, 33–34]. These diamond-shaped insulators and the sawtooth-shaped channel considered here all involve sharp corners, which can create strong gradients in the electric intensity and thus strong dielectrophoretic forces on particles. Thus the property of the electric field and its gradient near such sharp corners is of interest.

The electric field near a sharp corner is analyzed (see Appendix in Supportig Information) and the behavior of a particle near such a corner is summarized below, where α is the included angle of the corner as shown in Fig. 3:

$0<\alpha<2\pi/3$:	the corner is attracting and is a stagnation point;
$2\pi/3\leqslant\alpha<\pi$:	for negative DEP, the corner is attracting but not a stagnation point;
	for positive DEP, the corner is repelling;
$\pi<\alpha<2\pi$:	for negative DEP, the corner is repelling;
	for positive DEP, the corner is attracting.

These results are illustrated for a particle with negative DEP in Fig. 3, and they are used in conjunction with computations to understand particle movements in a sawtooth channel in Section 4.

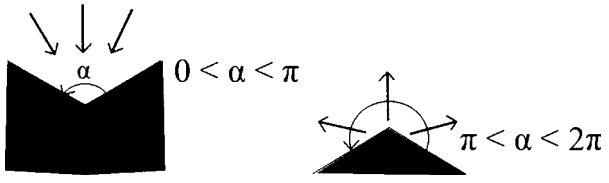

Figure 3. Behavior of a particle near a sharp corner for a particle with negative DEP.

3.3 Dielectrophoretic motion and saddle points

As shown in Eq. (3), the velocity of a particle is induced by electroosmosis of the fluid, particle electrophoretic motion and particle dielectrophoretic motion. Electroosmosis and electrophoretic velocities are proportional to the local electric field $\mathbf{E}$ while the dielectrophoretic velocity is proportional to $\nabla|\mathbf{E}|^2$. The dimensionless $(-\nabla|\mathbf{E}|^2)$ is plotted for $h_C = 1.0$, $h_T = 2.0$ in Fig. 4. There are several important features of the vector field $\nabla|\mathbf{E}|^2$. The first feature is that the horizontal component of $\nabla|\mathbf{E}|^2$alternates its direction as one moves from the divergent part of a cell (defined as the space between two adjacent teeth) to the convergent part of the cell and *vice versa*. For negative DEP, the dielectrophoretic motion of a particle is in the negative direction of $\nabla|\mathbf{E}|^2$. Figure 4 shows that in the divergent part of the cell, the particle moves in the x-direction (positive x-component velocity) and in the convergent part of the cell, the particle moves in the negative x-direction. These two distinct zones are separated by a saddle point (hyperbolic fixed point), located along the centerline (*e.g.* point B1). At a saddle point, $\nabla|\mathbf{E}|^2 = 0$, which is a stationary point but not a local extremum. A saddle point divides the $\nabla|\mathbf{E}|^2$ lines into four distinct branches. For negative DEP, particles move from $|\mathbf{E}|^2$ maximum at the tips of the teeth to $|\mathbf{E}|^2$ minimum at the bottom vertices at the base of the teeth. There are 13 such saddle points along the centerline in the seven-cell sawtooth channel and they act like barriers so that particles cannot travel from one zone to another based on dielectrophoretic motion *alone*. These barriers can be overcome only when the combined electroosmosis and electrophoretic effects are stronger than the opposing dielectrophoretic effect.

4 Particle trapping criteria in a sawtooth channel

As discussed previously, only particles with positive charge can enter the channel when the electric current is in the positive

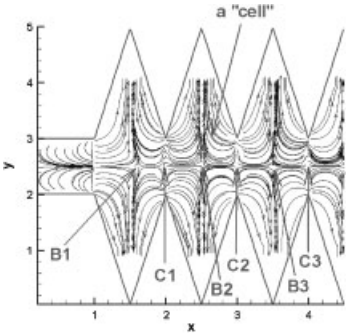

Figure 4. Plots of normalized $(-\nabla|\mathbf{E}|^2)$ in a seven-teeth sawtooth channel (only the first three 1/2 teeth are shown) for $h_c = 1.0$, $h_T = 2.0$. Points B1, C1 are saddle points with different properties: near B1, particles are pushed toward the sides of the channel, and near C1 particles are pushed toward the centerline. Points (B2, C2), (B3, C3) are similar to points (B1, C1). A ''cell'' is defined as the space between two teeth.

x-direction. In what follows, we shall focus on the movements of particles with negative DEP ($C>0$). Our objective is to establish a criterion under which particles with different properties can be separated by virtue of selectively blocking and trapping one type of particle within the basic unit while other types of particles pass through this unit completely. Note that, in a functional device, the sawtooth structures can be combined to trap various particles. Since the motion of a particle is completely characterized by Eq. (7), this blocking criterion is fully specified by the dimensionless parameter C, once the geometric parameters h_T, h_C and n are prescribed. Thus the different types of particles referred here are characterized by the parameter C, which is in essence a measure of the strength of dielectrophoretic force relative to the electrophoretic force acting on the particle. In this paper, we limit our study to seven teeth: $n = 7$ and $h_C = 1.0$, with $h_T = 2.0$ or 1.0.

We start with the geometry $h_T = 2.0$. At low values of C, dielectrophoretic effect is relatively weak and a particle will pass the unit completely regardless of its initial position at the entrance of the channel. Near the entrance of the channel, the repelling corner A elevates particles by forming a bump and pushes the particles toward the centerline (Fig. 5A). Similar repelling effects are observed near tips B and C, where ridges are formed in the particle pathlines. This is due to the repelling property of the sharp corners analyzed in Section 3.2. A further increase in the strength of the dielectrophoretic parameter C to 4.0 makes the particle pathlines even more sinuous, and the existence of saddle points in the particle pathlines becomes apparent (S1, S2 in Fig. 5B). These saddle points divide the nearby pathlines into four separate zones. Owing to symmetry, saddle points appear in pairs, with one on each side of the channel centerline. For $C = 4.0$, all particles started from the channel entrance still pass the sawtooth unit completely. Structural changes occur as the value of C is further increased. At $C = 6.5$, strong dielectrophoretic effect emanating from the sharp corners focuses the particles to the centerline (Fig. 5C). At $C = 7.0$, a wall-like structure appears near the exit (Fig. 5D). A line plot for the velocity of a particle traveling along the centerline shows that this ''wall'' structure brings down the particle velocity significantly as the particle moves toward the ''wall'' (Fig. 5E). The particle velocity, however, remains positive immediately after the particle past the ''wall''. Thus the appearance of the wall-like structure in particle pathlines does not necessarily block the motions of particles toward the unit exit.

When the value of C is further increased to 14, the two symmetrical saddle points on the two sides of the channel centerline are squeezed toward the centerline and they nearly coalesce (Fig. 6A). This repels particles near the centerline to the sides of the centerline, toward the valley of the cell. The reverse velocity zones behind the saddle point then seizes the *entire* cross section of the channel. Thus, no particles can travel across this barrier and particle blocking occurs. The velocity of a particle traveling along the centerline for $C = 14$ is shown in Fig. 6B. There are many wall-like structures in the particle pathlines for this high value of C. The particle velocity experiences a spike near every wall-like structure: the velocity is brought down dramatically when it hits the ''wall'', and it spikes back up as soon as it crosses the ''wall''. An example of this behavior is near $x = 7$. No reverse velocity occurs near $x = 7$, however, and the particle continues to move in the x-direction. Near $x = 7.8$, the velocity along the centerline first

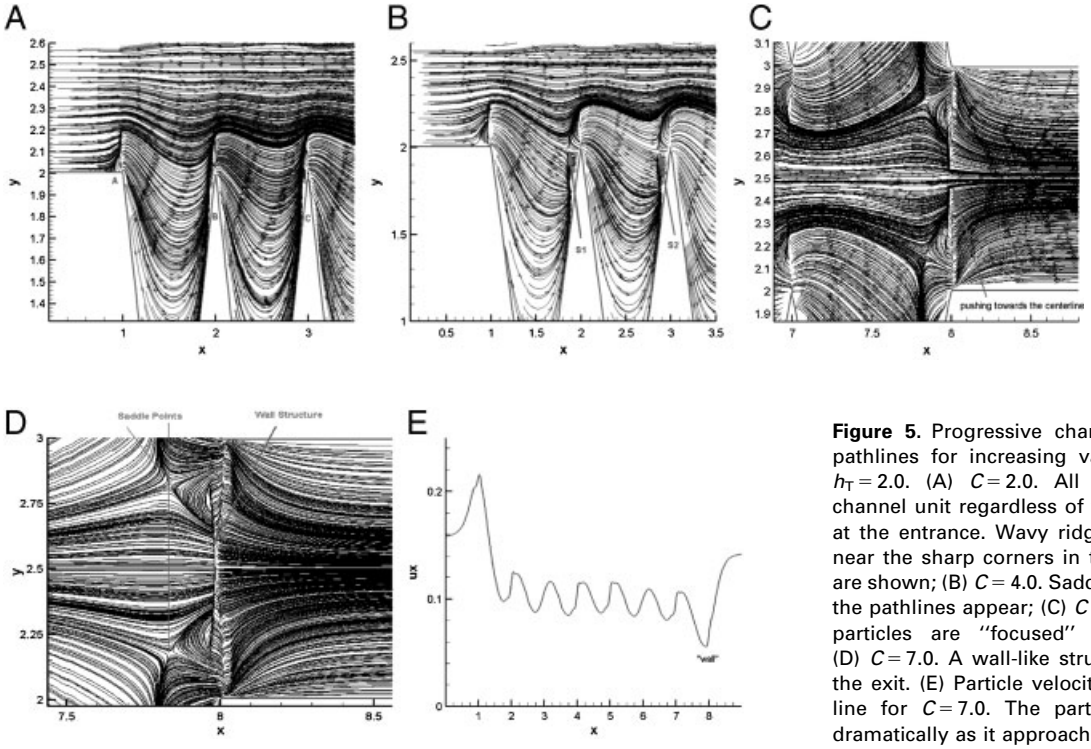

Figure 5. Progressive change in the particle pathlines for increasing value of C. $h_c = 1.0$, $h_T = 2.0$. (A) $C = 2.0$. All particles pass the channel unit regardless of their initial position at the entrance. Wavy ridges in the pathlines near the sharp corners in the entrance region are shown; (B) $C = 4.0$. Saddle points (S1, S2) in the pathlines appear; (C) $C = 6.5$. Near the exit, particles are ''focused'' to the centerline. (D) $C = 7.0$. A wall-like structure appears near the exit. (E) Particle velocity along the centerline for $C = 7.0$. The particle velocity drops dramatically as it approaches the ''wall''.

drops to zero at the saddle point and it then becomes negative, with a reverse velocity zone lying between $x = 7.8$ and 8. Thus, particles can no longer move past the cross section near $x = 7.8$. The coalescence of the two saddle points from the two sides of the centerline followed by the complete seizure of the cross section by a reverse velocity zone characterizes the blocking and the trapping of the particles.

The critical value of C for blocking the motion of a particle for the geometry $h_C = 1.0$, $h_T = 2.0$ is $C = 14$. Thus particles with $C < 14$ will pass this unit completely, regardless of their initial positions at the entrance, and particles with $C \geq 14$ will be prevented from passing through this unit. Therefore, a single sawtooth channel unit of this geometry successfully separates all particles into two groups, one with $C < 14$ and another with $C \geq 14$. Similar computations were performed for $h_C = 1.0$ but $h_T = 1.0$, which has relatively shallower valleys compared with the geometry with $h_T = 2.0$. As in the case of $h_T = 2.0$, the two distinct features are the appearance of wall-like structures and the squeezing of the saddle points toward the centerline as the dielectrophoretic effect becomes stronger (increasing C value). Only when the two symmetrical saddle points on the two sides of the centerline coalesce followed by a reverse velocity zone over the entire cross section that particles will be blocked and trapped. Again this first occurs near the exit of the channel unit, near $x = 8$. The critical value for this shallower channel is $C = 18$ *versus* $C = 14$ for $h_T = 2.0$. This larger critical value reflects the weaker dielectrophoretic effect in this geometry compared with $h_T = 2.0$, which has a deeper valley. Similarly we can tune the strength of the dielectrophoretic effects by changing h_C while holding a constant value of h_T.

We also carried out a study on a *sinusoidal* channel with seven periods. The only difference between this geometry and that of the sawtooth channel with $h_C = 1.0$, $h_T = 2.0$, is that the sharper corners have been smoothed out. The wall-like structures in particle pathlines at large values of C observed in sawtooth channels disappeared, and particles traveling along the centerline no longer experience velocity spikes (Fig. 7). Thus, wall-like structures in particle pathlines and velocity spikes are characteristics only for geometries with sharp corners. We also found that the critical value of C is 17 for the sinusoidal channel, which is much higher than 14 for the sawtooth channel as a consequence of weaker dielectrophoretic effect (sharp corners induces stronger dielectrophoretic effect). As in the sawtooth channel, this critical condition occurs when two saddle points on the opposite side of the centerline coalesce, with a reverse velocity zone occupying the entire channel cross section (near $x = 8$ in Fig. 7).

The above examples demonstrated that once the geometric aspect ratios h_C, h_T and n are specified for a sawtooth channel unit, particle blocking is determined by the dimensionless parameter C: there is a critical value C_r, so that when $C \geq C_r$ particles will be blocked. For $h_C = 1.0$, $h_T = 2.0$, $C_r = 14$, and for $h_C = 1.0$, $h_T = 1.0$, $C_r = 18$. Since C is defined by Eq. (8), for any particle with a mobility ratio $\mu_{DEP}/\mu_{EO}+\mu_{EM}$, we can always block the passage of this particle by varying the voltage across the channel unit $\Delta\Phi_0$, or by varying the spacing between the teeth L, or a combination of both, so that the resulting value of C is greater than the critical value for particle blocking for this sawtooth unit. In other words, an elementary unit of the sawtooth channel alone is capable of blocking any particle.

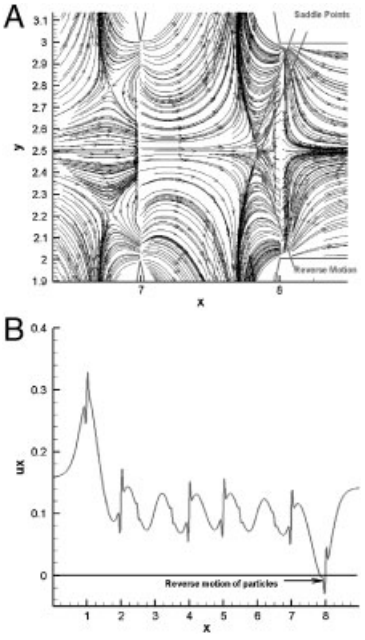

Figure 6. The critical condition for blocking particles. $h_c = 1.0$, $h_T = 2.0$ and $C = 14$. (A) Two saddle points on the two sides of the centerline move very close to each other near the centerline and nearly coalesce. This diverts all particle pathlines toward the valley of the channel. Reverse motion zones fill up the entire cross-section behind the saddle points. No particle can move past this barrier; (B) velocity of a particle travelling along the centerline at the critical condition. Velocity spikes near every "wall" and reverse motion of the particle occurs near $x = 8$.

If a device is constructed with a sawtooth unit with $h_T = 1.0$ and another unit with $h_T = 2.0$ connected sequentially, then this device will block particles with $C > 18$ in the first segment with $h_T = 1.0$, and particles with $14 < C < 18$ will be trapped in the sequential segment with $h_T = 2.0$. At the mean time, particles with $C < 14$ pass this two-segment device completely. To trap particles with smaller values of C, stronger gradient in the electric field is required. In this case, stronger gradient is created by a deeper valley in the sawtooth structure. We can easily add another segment in the device with even stronger electric field gradient to trap certain particles with $C < 14$, say, $10 < C < 14$. This exercise is equivalent to separating particles with different mobility ratios $(\mu_{DEP}/\mu_{EO}+\mu_{EM})$ (this ratio is *dimensional*), if the voltage drop and teeth spacing are the same for these two different units. It is thus possible to separate very similar particles by simply adjusting geometric parameters for these basic sawtooth units and connect them in a series to build a device. In the ultimately limit, we can adjust each cell, so that a spectrum of similar particles can be separated in a continuous manner, as in the converging sawtooth channel used in [39]. In this case, each cell will trap a different particle.

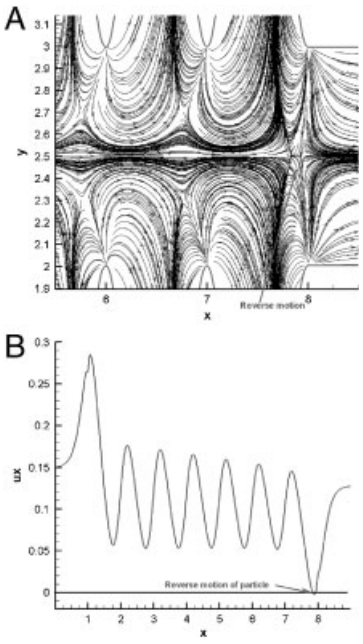

Figure 7. Particle pathlines in a sinusoidal channel with the same valley depth as $h_c = 1.0$, $h_T = 2.0$ and $C = 17$. (A) No wall-like structures appear in the particle pathlines. Blockage occurs when symmetrical saddle points nearly coincide near the centerline and reverse motion zone occupies the entire cross section near $x = 8$; (B) velocity of a particle travelling along the centerline. No spikes in the particle velocity occur due to the absence of the ''wall'' structure in the particle pathlines. A small reverse motion zone occurs near $x = 8$. Particles are blocked within the unit.

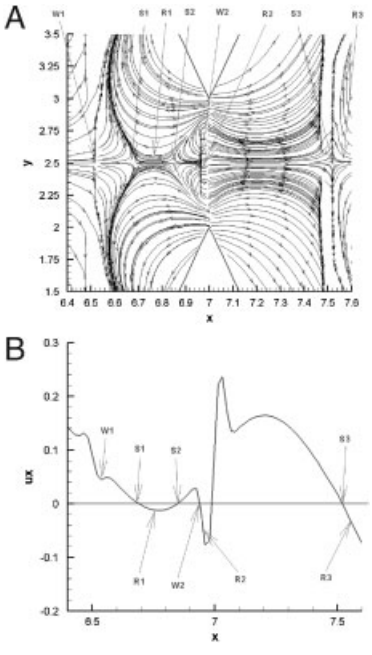

Figure 8. Particle pathline structures for $h_c = 1.0$, $h_T = 2.0$ and $C = 50$. (A) ''Walls'', saddle points, ''reverse flow zones'' are indicated by the letters ''W'', ''S'' and ''R'', respectively; (B) velocity of a particle travelling along the centerline. The markers correspond to the points and zones in (A).

5 Further discussion on particle pathline structures in sawtooth channels

As discussed previously, the appearance of DEP wall-like structures in particle pathlines and the velocity spikes near such a structure are common features of particle motion in a sawtooth channel when dielectrophoretic effect is strong (large values of C). To delineate the details of such features, a computation was carried out for $h_c = 1.0$, $h_T = 2.0$ and $C = 50$. Only the sections from $x = 6.4$ to 7.6 are shown in Fig. 8. In this section of the unit, there are two DEP ''walls'', one near $x = 6.52$ and another near $x = 6.95$ (''W1'' and ''W2'' in Fig. 8A). For a particle travelling along the centerline, its velocity experiences a sharp decrease as it moves toward W1 at $x = 6.52$. The particle velocity reaches a local minimum when the particle reaches W1 at $x = 6.52$. The velocity remains positive, however. It then resumes its decrease as the particle moves toward the saddle point S1 at $x = 6.65$, at which point, the velocity becomes zero (Fig. 8B). A reverse velocity zone follows, as the velocity dips below zero (R1). Another saddle point S2 appears near $x = 6.85$ and the velocity recovers to zero. It becomes positive for a short distance before it drops back to zero again at W2 near $x = 6.95$. A very short reverse velocity zone exists immediately after this wall (R2), which makes this wall different from wall W1 at $x = 6.52$. The velocity then spikes back to positive after this narrow reverse velocity zone and remains positive till the particle reaches the saddle point S3 near $x = 7.5$. Another reverse velocity zone appears after $x = 7.5$. Note that not all saddle points are equal: S1 and S3 are followed by reverse velocity zones while S2 is not; not all DEP ''walls'' are the same: wall W2 is followed by a reverse velocity zone and wall W1 is not.

This detailed study further enforces the revelation that there are rich structures in particle pathlines when dielectrophoretic effect is strong, which corresponds to large values of C. These salient features include DEP wall-like structures and the associated spikes in particle velocity; the coalescence of symmetric saddle points onto the centerline, which may or may not be followed by a reverse velocity zone. Blockage of particle motion occurs only when a reverse velocity zone occupies an entire cross section of the channel.

6 Concluding remarks

In this paper, we studied particle movements in a non-converging sawtooth channel in detail. Certain salient features of the particle pathlines are found, in particular wall-like structures, velocity spikes and saddle points. The DEP wall-like structures and velocity spikes are characteristic for channels with sharp corners only. Particle blockage occurs only when the symmetrical saddle points on the two sides of the centerline coalesce onto the centerline followed by a reverse velocity zone occupying the entire channel cross section. It is shown that a single dimensionless parameter $C(= (\mu_{DEP})/(\mu_{EO} + \mu_{EM})\Delta\Phi_0/L^2)$ can be used to establish such a particle blocking condition for a single basic channel unit when dimensionless geometric parameters are specified. Sharp

corners are beneficial to separation since the critical value of C for blockage is lower than channels with smooth corners. Combining units with different geometric properties in a series can be used to selectively block and trap particles with different properties. The study indicates that the basic channel unit can be further simplified to contain only one cell (instead of seven used in this paper) and a channel with multiple cells of progressively stronger field gradient can be built and tuned geometrically to separate diverse particle mixture. This confirms the principle illustrated experimentally by Pysher and Hayes [39]. If two particles have nearly identical values of mobility ratio$\mu_{DEP}/\mu_{EO}+\mu_{EM}$, we can always adjust the value of $\Delta\Phi_0/L^2$ so that the difference in the respective values of parameter C for these two particles is significant. This will then allow these two particles to be separated easily using the sawtooth channel device. Thus it can be argued that the resolution of this type of device can be tuned to any desired level. It is expected that further investigations combined with experiments with well-characterized particles in the future will drive home the idea of continuously separation using sawtooth channels.

Computational resources for this work were provided by the Ira A. Fulton High Performance Computing Initiative at ASU.

The authors have declared no conflict of interest.

7 References

[1] Pohl, H. A., *J. Appl. Phys.* 1951, *22*, 869–871.

[2] Pohl, H. A., *Dielectrophoresis*, Cambridge University Press, Cambridge 1978.

[3] Washizu, M., Jones, T. B., *J. Electrostat.* 1994, *33*, 187–198.

[4] Jones, T. B., *J. Electrostat.* 1979, *6*, 69–82.

[5] Jones, T. B., *J. Electrostat.* 1986, *18*, 55–62.

[6] Jones, T. B., *Electromechanics of Particles*, Cambridge University Press, New York 1995.

[7] Jones, T. B., Washizu, M., *J. Electrostat.* 1996, *37*, 121–134.

[8] Becker, F. F., Wang, X. B., Huang, Y., Pethig, R., Vykoukal, J., Gascoyne, P. R. C., *Proc. Natl. Acad. Sci. USA* 1995, *92*, 860–864.

[9] Gascoyne, P., Mahidol, C., Ruchirawat, M., Satayavivad, J., Watcharasit, P., Becker, F. F., *Lab Chip* 2002, *2*, 70–75.

[10] Huang, Y., Ewalt, K. L., Tirado, M., Haigis, R., Foster, A., Ackley, D., Heller, M. J. *et al.*, *Anal. Chem.* 2001, *73*, 1549–1559.

[11] Huang, Y., Wang, X. B., Becker, F. F., Gascoyne, P. R. C., *Biochim. Biophys. Acta* 1996, *1282*, 76–84.

[12] Green, N. G., Morgan, H., *J. Phys. D Appl. Phys.* 1998, *31*, L25–L30.

[13] Green, N. G., Morgan, H., Milner, J. J., *J. Biochem. Biophys. Methods* 1997, *35*, 89–102.

[14] Markx, G. H., Talary, M. S., Pethig, R., *J. Biotechnol.* 1994, *32*, 29–37.

[15] Morgan, H., Green, N. G., *J. Electrostat.* 1997, *42*, 279–293.

[16] Morgan, H., Hughes, M. P., Green, N. G., *Biophys. J.* 1999, *77*, 516–525.

[17] Pethig, R., *Crit. Rev. Biotechnol.* 1996, *16*, 331–348.

[18] Pethig, R., Huang, Y., Wang, X. B., Burt, J. P. H., *J. Phys. D Appl. Phys.* 1992, *25*, 881–888.

[19] Ramos, A., Morgan, H., Green, N. G., Castellanos, A., *J. Phys. D Appl. Phys.* 1998, *31*, 2338–2353.

[20] Wang, X. B., Huang, Y., Burt, J. P. H., Markx, G. H., Pethig, R., *J. Phys. D Appl. Phys.* 1993, *26*, 1278–1285.

[21] Wang, X. B., Huang, Y., Gascoyne, P. R. C., Becker, F. F., Holzel, R., Pethig, R., *Biochim. Biophys. Acta* 1994, *1193*, 330–344.

[22] Gascoyne, P., Pethig, R., Satayavivad, J., Becker, F. F., Ruchirawat, M., *Biochim. Biophys. Acta* 1997, *1323*, 240–252.

[23] Cheng, J., Sheldon, E. L., Wu, L., Heller, M. J., O'Connell, J. P. *Anal. Chem.* 1998, *70*, 2321–2326.

[24] Durr, E., Yu, J. Y., Krasinska, K. M., Carver, L. A., Yates, J. R., Testa, J. E., Oh, P., Schnitzer, J. E., *Nat. Biotechnol.* 2004, *22*, 985–992.

[25] Fiedler, S., Shirley, S. G., Schnelle, T., Fuhr, G., *Anal. Chem.* 1998, *70*, 1909–1915.

[26] Hunt, T. P., Lee, H., Westervelt, R. M., *Appl. Phys. Lett.* 2004, *85*, 6421–6423.

[27] Minerick, A. R., Zhou, R. H., Takhistov, P., Chang, H. C., *Electrophoresis* 2003, *24*, 3703–3717.

[28] Wang, X. B., Huang, Y., Wang, X. J., Becker, F. F., Gascoyne, P. R. C., *Biophys. J.* 1997, *72*, 1887–1899.

[29] Wong, P. K., Chen, C. Y., Wang, T. H., Ho, C. M., *Anal. Chem.* 2004, *76*, 6908–6914.

[30] Cummings, E. B., Singh, A. K., *Anal. Chem.* 2003, *75*, 4724–4731.

[31] Lapizco-Encinas, B. H., Simmons, B. A., Cummings, E. B., Fintschenko, Y., *Electrophoresis* 2004, *25*, 1695–1704.

[32] Kwon, J. S., Maeng, J. S., Chun, M. S., Song, S., *Microfluid. Nanofluidics* 2008, *5*, 23–31.

[33] Lapizco-Encinas, B. H., Simmons, B. A., Cummings, E. B., Fintschenko, Y., *Anal. Chem.* 2004, *76*, 1571–1579.

[34] Barrett, L. M., Skulan, A. J., Singh, A. K., Cummings, E. B., Fiechtner, G. J., *Anal. Chem.* 2005, *77*, 6798–6804.

[35] Kang, K. H., Kang, Y. J., Xuan, X. C., Li, D. Q. *Electrophoresis* 2006, *27*, 694–702.

[36] Kang, K. H., Xuan, X. C., Kang, Y. J., Li, D. Q. *J. Appl. Phys.* 2006, *99*.

[37] Kralj, Jason G., Lis, Michael T. W., Schmidt, Martin A., Jensen, Klavs F., *Anal. Chem.* 2006, *78*, 5019–5025.

[38] Gascoyne, P., Vykoukal, J. *Electrophoresis* 2002, *23*, 1973–1983.

[39] Pysher, M. D., Hayes, M. A., *Anal. Chem.* 2007, *79*, 4552–4557.

[40] Kadaksham, A. T. J., Singh, P., Aubry, N., *Electrophoresis* 2004, *25*, 3625–3632.

[41] Aubry, N., Singh, P., *Europhys. Lett.* 2006, *74*, 623–629.

[42] Pacheco, J. R., *Int. J. Numer. Methods Fluids* 2001, *35*, 71–91.

[43] Pacheco, J. R., Peck, R. E., *Numer. Heat Transfer* 2000, *Part B 37*, 267–291.

